

Bifunctional Sphingosine for Cell-Based Analysis of Protein-Sphingolipid Interactions

Per Haberkant*,†,‡ Frank Stein,† Doris Höglinder,† Mathias J. Gerl,‡ Britta Brügger,‡
Paul P. Van Veldhoven,§ Jeroen Krijgsveld,|| Anne-Claude Gavin,|| and Carsten Schultz*,†

[†]European Molecular Biology Laboratory, Cell Biology and Biophysics Unit, Meyerhofstr. 1, 69117 Heidelberg, Germany

[‡]Heidelberg University Biochemistry Center, Im Neuenheimer Feld 328, 69120 Heidelberg, Germany

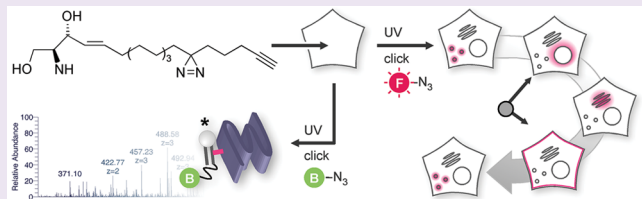
[§]Laboratory for Lipid Biochemistry and Protein Interactions, Department of Cellular and Molecular Medicine, KU Leuven, B-3000 Leuven, Belgium

^{||}European Molecular Biology Laboratory, Genome Biology Unit, Meyerhofstr. 1, 69117 Heidelberg, Germany

[¶]European Molecular Biology Laboratory, Structural and Computational Biology Unit, Meyerhofstr. 1, 69117 Heidelberg, Germany

Supporting Information

ABSTRACT: Sphingolipids are essential structural components of cellular membranes and are crucial regulators of cellular processes. While current high-throughput approaches allow for the systematic mapping of interactions of soluble proteins with their lipid-binding partners, photo-cross-linking is the only technique that enables for the proteome-wide mapping of integral membrane proteins with their direct lipid environment. Here, we report the synthesis of a photo-activatable and clickable analog of sphingosine (pacSph). When administered to sphingosine-1-phosphate lyase deficient cells, pacSph allows its metabolic fate and the subcellular flux of *de novo* synthesized sphingolipids to be followed in a time-resolved manner. The chemoproteomic profiling yielded over 180 novel sphingolipid-binding proteins, of which we validated a number, demonstrating the unique value of this technique as a discovery tool. This work provides an important resource for the understanding of the global cellular interplay between sphingolipids and their interacting proteins.



Biological membranes of mammalian cells consist of thousands of different lipids, of which the majority can be assigned to one of the three major lipid classes: glycerolipids, sterols and sphingolipids.¹ In addition to their function as structural components of biomembranes, sphingolipids are components of specialized membrane domains that may or may not be enriched with cholesterol.^{2–6} Apart from these structural features, sphingolipids are involved in central cell-signaling pathways such as the regulation of cell proliferation, apoptosis, senescence, and intracellular trafficking.⁷ Any alteration of these processes is believed to be associated with pathologies. Not surprisingly, derailed sphingolipid homeostasis is linked to diseases such as cancer, diabetes, and metabolic syndrome.^{8,9} Apart from the machinery required for their biosynthesis, only a few proteins have been reported to directly interact with sphingolipids.^{8,10,11} In fact, one of the major “voids” in our knowledge of function of bioactive sphingolipids derives from the paucity of understanding how they work and what proteins they interact with. This is mainly due to a lack of tools that allow for a systematic mapping of protein-sphingolipid interactions. The latter especially applies to interactions of membrane spanning proteins within their native environment. In 2010, the first sphingosine 1-phosphate (S1P) receptor modulator, fingolimod (FTY720), was approved as a therapeutic for multiple sclerosis, demonstrating the impor-

tance of protein-sphingolipid complexes as potential therapeutic targets.¹² We and others have demonstrated the use of photoactivatable and clickable (pac) lipids for the *in vivo* identification of protein–lipid interactions.^{13–16} Here, we expand this technology to the class of sphingolipids. Aiming for the visualization and proteomic profiling of protein–sphingolipid complexes in living cells, we synthesized a bifunctional sphingosine (pacSph) with the following two features: (i) a photoactivatable diazirine ring for the UV-light induced covalent linkage of photoactivatable sphingolipids to proteins in close proximity and (ii) a terminal alkyne moiety that allows for the subsequent tagging of protein–lipid complexes by click chemistry. We demonstrate its application for monitoring the *de novo* synthesis of sphingolipids and the imaging of their intracellular flux. Further, we employed pacSph for the chemoproteomics profiling of sphingolipid handling machinery and for validating several novel sphingolipid-binding proteins.

Received: August 5, 2015

Accepted: November 11, 2015

Published: November 11, 2015



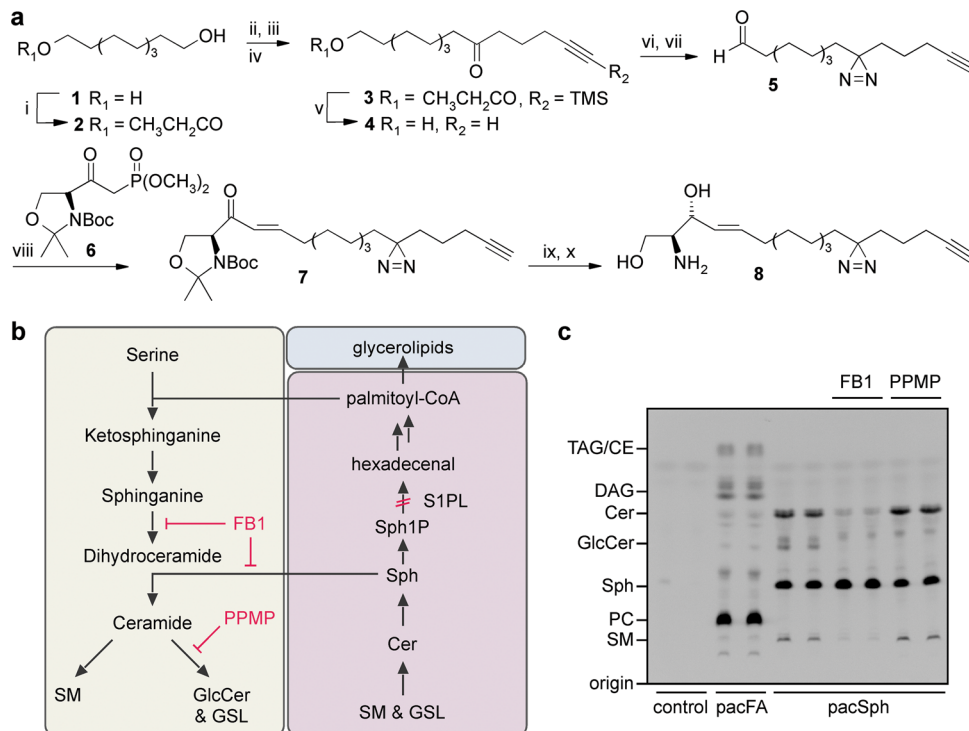


Figure 1. Synthesis and metabolic fate of bifunctional sphingosine (pacSph, 8). (a) (i) $\text{CH}_3\text{CH}_2\text{COOH}$, p-toluenesulfonic acid, reflux, 40%; (ii) oxalyl chloride, DMSO, Et_3N , 81%; (iii) $\text{Mg}, \text{Cl}(\text{CH}_2)_3\text{CCTMS}$, -20°C , 57%; (iv) oxalyl chloride, DMSO, Et_3N , 92%; (v) 2 M KOH/MeOH, 50°C , 97%; (vi) $\text{NH}_3, \text{H}_2\text{NOSO}_3\text{H}, \text{I}_2$, 18%; (vii) oxalyl chloride, DMSO, Et_3N , 89%; (viii) oxazolidin 13, $\text{K}_2\text{CO}_3, \text{ACN}/\text{H}_2\text{O}$, 45°C , 64%; (ix) $\text{NaBH}_4, \text{CeCl}_3, \text{MeOH}$, 42%; (x) HCl, MeOH , 50°C , 90%. (b) Simplified representation of the biosynthesis (highlighted in yellow) and degradation (highlighted in red) of sphingolipids. Fumonisin B1 (FB1) inhibits the conversion of sphinganine and sphingosine (Sph) to ceramide (Cer); 1-phenyl-2-palmitoyl-3-morpholino-1-propanol (PPMP) inhibits the glucosylceramide (GlcCer) synthase. (c) Analysis of lipid extracts from S1PL^{-/-} cells that were fed with pacFA or pacSph for 1 h in the absence or presence of fumonisin B1 (FB1) or 1-phenyl-2-palmitoyl-3-morpholino-1-propanol (PPMP). Lipid extracts were subjected to click reactions with coumarin azide, separated by TLC and analyzed by fluorescence imaging. Abbreviations: SM, sphingomyelin; GSL, glycosphingolipid; TAG, triacylglycerol; CE, cholesterol ester.

RESULTS AND DISCUSSION

Synthesis of Bifunctional Sphingosine. The bifunctional sphingosine (pacSph 8, Figure 1a) was designed such that its chemical structure closely mimicked that of its natural counterpart. For the synthesis, we therefore followed the design of a previously reported and applied photoactivatable sphingosine,¹⁷ complicated by the need to accommodate a clickable alkyne group. For its total synthesis, the mono-propionoylated 1,2-decanediol 2 was oxidized to the aldehyde and, after a Grignard reaction with TMS-protected 5-chloro-1-pentynyl, provided ketone 3. Protecting groups were removed, and the resulting compound 4 was converted to the photoactivatable diazirine in a three-step reaction and further to aldehyde 5. The sphingoid backbone 7 was then assembled in a Wadsworth–Horner–Emmons reaction with oxazolidine 6. Non-stereospecific reduction and deprotection of 7 yielded pacSph (8).

Metabolic Fate of pacSph. To investigate whether pacSph serves as a precursor for the biosynthesis of other sphingolipids, we followed the metabolic fate of pacSph in HeLa cells. For comparison, we used a C15-carbon long photoactivatable and clickable fatty acid (pacFA, Figure S1a) that was previously shown to give rise to bifunctional glycerolipids but not sphingolipids.¹³ Both precursors were fed to HeLa cells; lipid extracts were obtained and subjected to click reactions with the fluorogenic dye 3-azido-7-hydroxycoumarin (coumarin azide) followed by analysis via thin layer chromatography (TLC) as described previously.¹⁸ Lipid extracts of cells that were cultured

in the absence of clickable lipid precursors served as controls. Although pacFA and pacSph gave rise to different subsets of alkyne containing lipids, both precursors were predominantly incorporated into the glycerolipid phosphatidylcholine (PC; Figure S1b).¹³ This is in line with previous studies employing radioactive or fluorescent-labeled sphingosine that, like pacSph, were found to rapidly degrade and incorporate into glycerolipids, mainly PC and phosphatidylethanolamine.^{19,20} In comparison with recently described fluorescent Sph,¹⁹ we found pacSph to be predominantly incorporated into glycerolipids, which might be due to the different cell line and feeding conditions used. Incorporation of pacSph into glycerolipids can be explained by the fact that Sph is not only a precursor for sphingolipid biosynthesis, but it is also an intermediate in their native catabolism (Figure 1b). Phosphorylation by the Sph kinases (SK) yields sphingosine 1-phosphate (S1P), which can irreversibly be cleaved at sphingoid backbone by the action of the S1P lyase (S1PL).^{21–23} In this way, the sphingoid substrate escapes the sphingolipid anabolic pathway. The resulting degradation product 2-hexadecenal then enters the biosynthetic pathway for glycerolipids (Figure 1b).²⁴ In the following experiments, we made use of mouse embryonic fibroblasts (MEFs) derived from S1PL-deficient mice (S1PL^{-/-}) in order to prevent degradation of pacSph.²⁵ In this cell line, pacSph was not converted into glycerolipids and gave rise to different metabolites compared to pacFA-fed cells (Figure 1c). To investigate the metabolic fate of our modified Sph, cells were fed pacSph in the absence and presence of

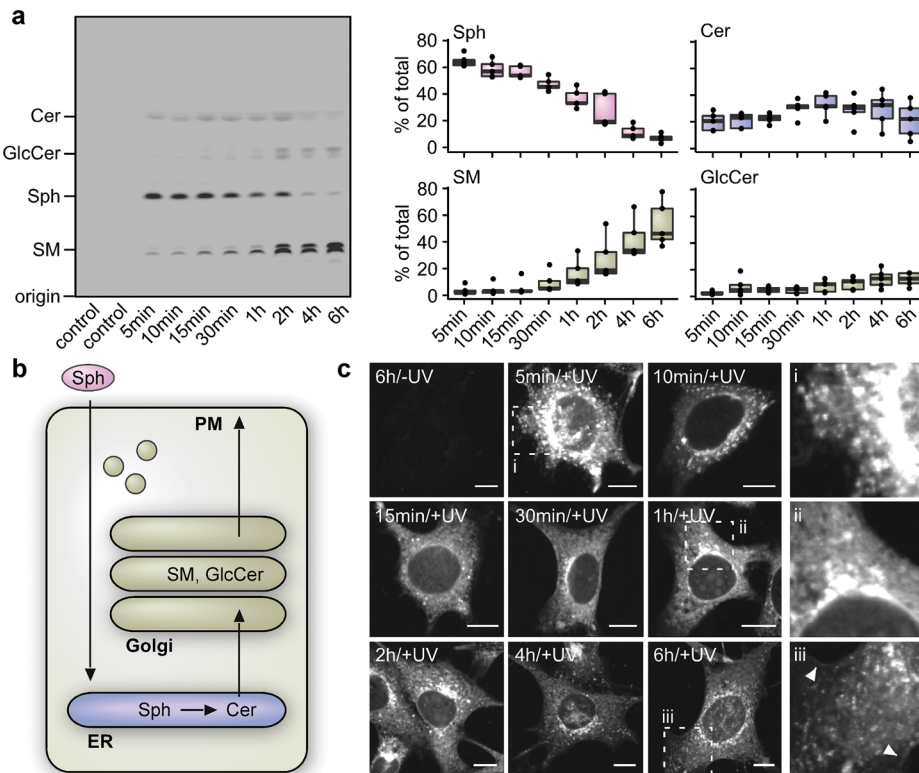


Figure 2. Metabolic fate of pacSph and imaging of protein–sphingolipid complexes. $S1PL^{-/-}$ MEFs were fed for 10 min with pacSph and then chased for the indicated time in the absence of pacSph. (a) Representative analysis of pacSph labeled lipids by TLC (left) and quantification of five independent experiments (right). (b) Schematic representation of sphingolipid biosynthesis. (c) Protein–sphingolipid complexes were captured by UV-light and then visualized by click reactions with Alexa 488 azide. (i–iii) Enlargement of the boxed area. Arrowheads indicate plasma membrane staining. Bar, 10 μ m.

fumonisin B1 (FB1) and PPMP, respectively.^{26,27} While FB1 inhibits ceramide (Cer) synthases (CERS), PPMP inhibits the glucosylceramide (GlcCer) synthase and therefore the biosynthesis of glycosphingolipids (GSLs; Figure 1b). We found that FB1 markedly decreased the *de novo* synthesis of all pacSph-derived metabolites and resulted in elevated intracellular pacSph levels (Figure 1c and Figure S2a). Furthermore, PPMP led to the decrease of two bands, presumably GlcCer species (Figure 1c and Figure S2a).

To further address the nature of different pacSph derived metabolites, lipid extracts derived from pacSph fed $S1PL^{-/-}$ cells were subjected to an enzymatic reaction employing a bacterial sphingomyelinase (SMase) prior to click reactions. SMase treatment led to a decreased intensity of the slowest and an increased intensity of the fastest migrating band, which were therefore assigned as bifunctional Cer and SM, respectively (Figure S2b). The suitability of pacSph as a precursor for the biosynthesis of sphingolipids was further supported by mass spectrometric analysis of lipid extracts derived from $S1PL^{-/-}$ MEFs that were fed with pacSph for 24 h. Masses showed a 36 Da increase in *m/z* ratios relative to endogenous sphingolipid species, corresponding to the higher mass of the photo-activatable and clickable sphingoid backbone. The identification of bifunctional SM 16:0, SM 24:1, multiple cerebroside-(HexCer 16:0, 18:0, 20:0, 22:0, 24:1, and 24:0), and higher glycosylated sphingolipid-species (LacCer 16:0, 18:0, 20:0, 22:0, 24:1, 24:0, and GM3 16:0, 18:0, 20:0, 22:0, 24:1) demonstrates the biocompatibility of pacSph for the *de novo* synthesis of bifunctionalized sphingolipids (Figure S3 and Figure S4). As ceramide synthases possess a high specificity

toward the acyl CoA chain length used for N-acylation, it is likely that various CERS are involved in the N-acylation of pacSph.²⁸ We conclude that feeding pacSph to $S1PL^{-/-}$ MEFs exclusively yielded bifunctional sphingolipid species, while pacFA gave rise to bifunctional glycerolipids.

Imaging of Protein–Lipid Complexes. In order to follow the flux of pacSph and its metabolites in time and space, we employed pacSph in pulse-chase experiments. To this end, $S1PL^{-/-}$ MEFs were cultured for 10 min in pacSph containing medium (pulse) and then chased in medium devoid of pacSph. Lipid extracts were subjected to click reactions with coumarin azide and analyzed by TLC (Figure 2a). The precursor pacSph decreased from initially 65% (5 min) of bifunctionalized lipids to less than 10% 6 h post chase. After 5 min, Cer was found to be the first metabolite formed (20%), indicating that pacSph reached the endoplasmic reticulum (ER) where CERS operate.²⁰ This is in accordance with the reported observation that Sph spontaneously translocates to the cytosolic side and equilibrates with intracellular membranes.²⁹ While Cer levels were kept nearly constant throughout the experiment, SM levels significantly increased from 30 min onward and reached up to 50% after 6 h. GlcCer levels were found to slightly increase starting from 1 h post chase, indicating that the Cer flux necessary for GlcCer formation had reached the Golgi.³⁰ Together, this demonstrates that pacSph is metabolized in a similar fashion like previously described radiolabeled photo-activatable sphingosine and its natural counterpart sphingosine.¹⁷

We then addressed whether the *in situ* visualization of protein–lipid complexes allows the flux of bifunctional

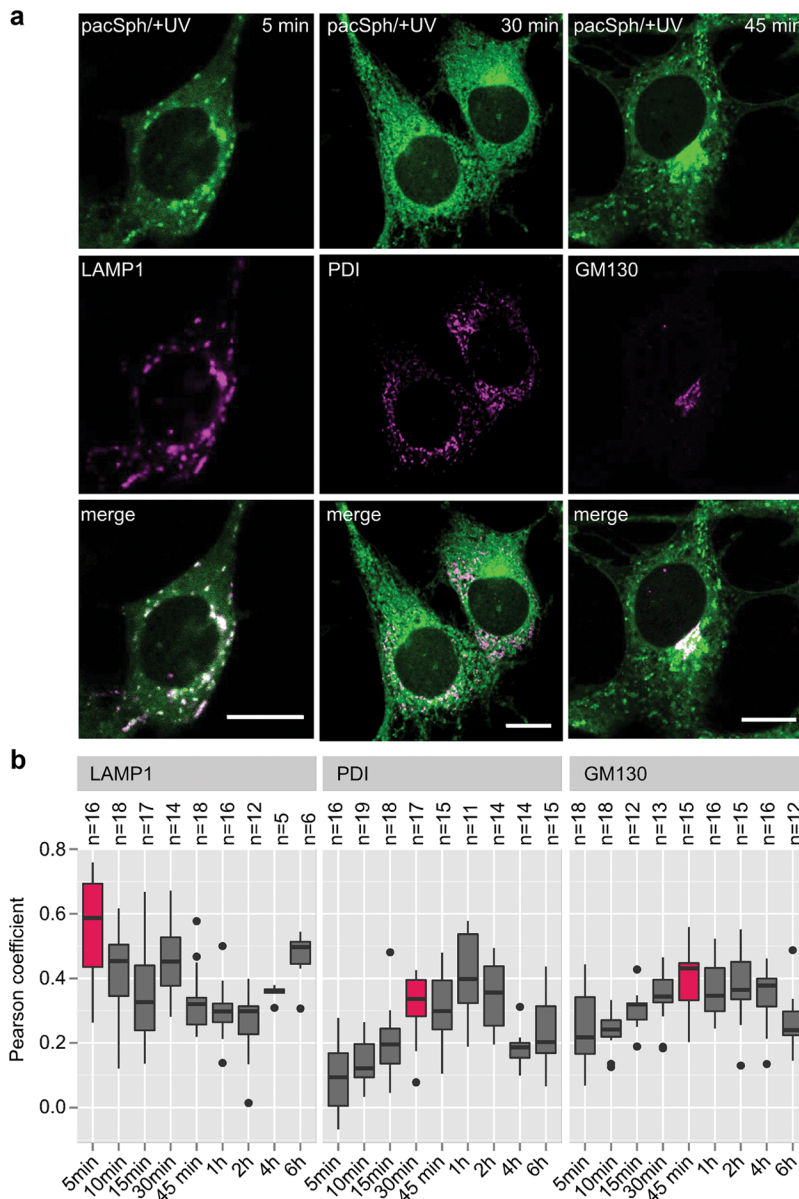


Figure 3. Time dependent colocalization of protein–sphingolipid complexes with different organelles. (a) $S1PL^{-/-}$ MEFs were fed for 10 min with 6 μ M pacSph and then chased in medium without pacSph for the indicated time. Cells were subjected to UV-irradiation, nonprotein bound lipids were extracted and protein–lipid complexes labeled by click reactions with Alexa 488 azide. Subsequently, cells were labeled with either anti-LAMP1, anti-PDI or anti-GM130. Shown are representative images of protein–sphingolipid complexes (green) and the respective organelle marker (magenta). Bar, 10 μ m. (b) Displayed are Pearson correlation coefficients, a measure for the colocalization of protein–sphingolipid complexes with LAMP1, PDI, and GM130 (quantification of at least 5 individual images ($n \geq 5$) displaying 6–16 cells per image. For each box plot, the top and bottom whiskers denote the maximum and minimum values. The top and bottom of the box indicates the 75th and 25th percentiles. The bold line denotes the 50th percentile. Outliers are plotted as individual points. Highlighted in red are data points shown in a.

sphingolipids to be followed within intact cells. $S1PL^{-/-}$ MEFs were pulse-chased, before protein–lipid complexes were captured by a flash of UV-light (≥ 345 nm). Cells were fixed with methanol at -20 °C, and non-protein bound lipids were removed by lipid extraction, to ensure that only covalently fixed lipids were visualized.¹³ Protein–sphingolipid complexes were subjected to click reactions with Alexa 488 azide and visualized by confocal microscopy (Figure 2c). In contrast to control cells that were fed for 6 h with pacSph but were not subjected to UV-irradiation, pacSph/+UV-treated cells showed a strong fluorescence staining. Interestingly, after a chase of 5 min, protein–sphingolipid complexes gave rise to a prominent staining of punctate structures that were found to colocalize

with the late endosomal/lysosomal marker LAMP1 (Figure 2c, Figure S5, and Figure 3). Within 15 min, we observed a decrease in the colocalization of protein–sphingolipid complexes with LAMP1 (Figure 3 and Figure S5), suggesting that pacSph has escaped the lysosomes. A total of 30 min post chase, protein–sphingolipid complexes gave rise to a homogeneous staining throughout the cells, which colocalized with PDI, a marker for the ER (Figure 2c, Figure 3, and Figure S6). In addition, protein–sphingolipid complexes colocalized with GM130, a marker for the trans-Golgi network (Figure 3 and Figure S7). Similar observations have previously reported employing fluorescent Sph.¹⁹ Colocalization of protein–sphingolipid complexes with GM130 was more pronounced

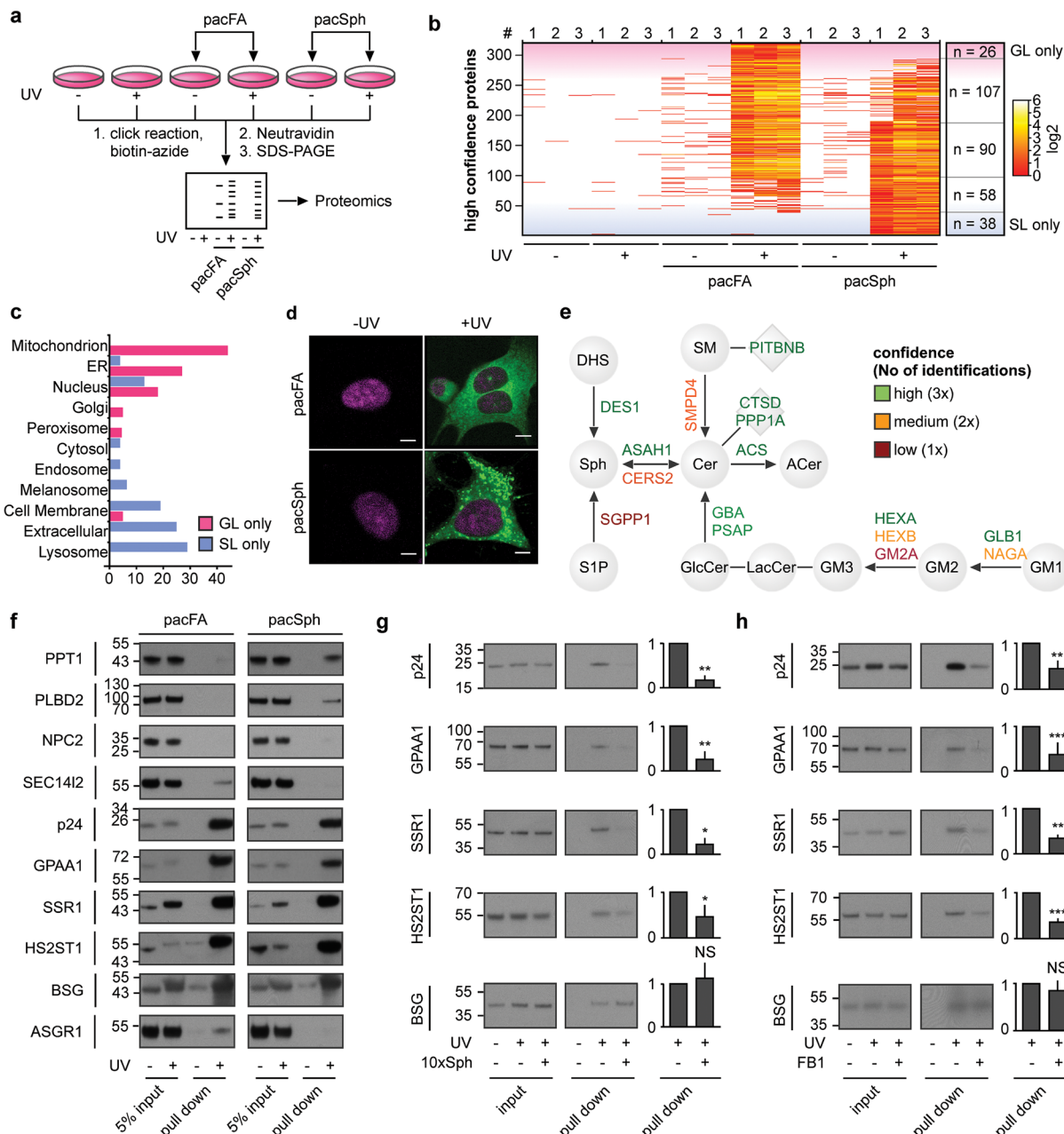


Figure 4. Global profiling of protein–lipid interactions in pacFA and pacSph-fed S1PL^{−/−} MEFs. a) Schematic representation of the identification of protein–lipid complexes.

Cells were cultured for 1 h in the absence or presence of either pacFA or pacSph and then subjected to UV-irradiation as indicated. Protein–lipid complexes were affinity-purified with Neutravidin beads after click reactions with biotin azide and analyzed by mass spectrometry. (b) Spectral counts of high confidence proteins identified from pacFA/+UV and pacSph/+UV treated cells are displayed as a heat map. (c) Localizations of high confidence proteins according to GO-annotations of proteins that were exclusively identified for pacFA/+UV (glycerolipids (GL) only) or pacSph/+UV (sphingolipids (SL) only) treated cells. (d) S1PL^{−/−} MEFs were fed for 1 h with pacFA or pacSph, subjected to UV-irradiation as indicated, and processed for the imaging of protein–lipid complexes. Nuclei were stained with Hoechst. Bars, μ m. (e) Overview of the sphingolipid biosynthetic pathway and sphingolipid handling machinery that was identified from pacSph/+UV treated S1PL^{−/−} MEF cells. Metabolites are displayed in circles. Transfer proteins and sphingolipid-regulated proteins are shown in squared boxes. Identified proteins are color coded as indicated. Arrows indicate the direction in which the proteins operate. (f) Experimental validation of sphingolipid-binding proteins. Proteins were transiently expressed in S1PL^{−/−} HeLa cells and fed for 4 h with pacFA or pacSph, subjected to UV-irradiation, click reactions with biotin-azide. Protein–lipid complexes were enriched (pull down) and analyzed by SDS-PAGE and Western blotting. (g) S1PL^{−/−} HeLa cells were fed 0.5μ M pacSph in the absence or presence of 5μ M sphingosine and samples were processed as described in f). (h) S1PL^{−/−} HeLa cells were cultured for 4 h in the absence or presence of 50μ M FB1 and subsequently fed for 4 h with 0.5μ M pacSph in the absence or presence of FB1. Samples were analyzed as in f. $n \geq 3$ biological replicates. All bar plots: mean plus SD. A Student's two-tailed *t* test was used to determine *P* values (**P* < 0.05, ***P* < 0.01, ****P* < 0.001, NS: not significant).

times gave rise to a more pronounced plasma membrane (PM) staining, where steady state levels of endogenous sphingolipids are reported to be the highest.³² The observed increase in the

at 45 min, which is in line with the observed time-dependent increase of SM, produced in the Golgi (Figure 2a,b and Figure 3),³¹ and persisted with chase times up to 4 h. Longer chase

times gave rise to a more pronounced plasma membrane (PM) staining, where steady state levels of endogenous sphingolipids are reported to be the highest.³² The observed increase in the

colocalization of protein–sphingolipid complexes with LAMP1 6 h post chase is likely caused by the endocytosis of the *de novo* synthesized bifunctional sphingolipids. Similar observations have been reported by the group of Kraft employing fluorescently labeled sphingosine.¹⁹ Of main importance, the described technology enables for the visualization of protein–lipid complexes. While allowing following the flux of pacSph and its metabolites through the cell, we like to point out that the technology does not allow for a quantitative comparison of the functionalized lipids among subcellular compartments.

Chemoproteomics Profiling of Protein–Lipid Complexes. Our observation that pacSph is recognized by the sphingolipid biosynthetic machinery prompted us to investigate pacSph for the proteome-wide identification of protein–sphingolipid complexes in living cells. In order to capture interactions throughout the cell rather than within particular subcellular localizations, we envisaged that continuous labeling would be preferred over pulse-chase labeling. We first analyzed the time dependent incorporation of pacSph into SLs when S1PL^{-/-} MEFs were cultured in the presence of pacSph (Figure S8a and b). When cells were fed pacSph for 1 h, similar levels of bifunctional SM (8%) and GlcCer (10%) were observed. At the same time, bifunctional Cer (20%) and pacSph (30%) levels were found at intermediate levels compared with longer (6 h) or shorter (30 min) incubation times. For the proteomic profiling of protein–lipid complexes, cells were cultured for 1 h in the absence or presence of either pacFA or pacSph. Under these conditions pacFA predominantly gave rise to PC (Figure 1b). Cells were subjected to UV irradiation. Total cell lysates were prepared, subjected to click reactions with biotin azide and the biotinylated complexes were enriched using Neutravidin beads (Figure 4a). For the analysis of protein–lipid complexes by in-gel fluorescence, analytical samples were subjected to click reactions with Alexa 488 azide and separated by SDS-PAGE (Figure S8c). Subsequent Coomassie staining showed that photoaffinity labeled proteins were distinct from the most abundant proteins. A comparison of pacFA/+UV with pacSph/+UV treated cells revealed proteins predominantly labeled for either treated cells. Although different subsets of bifunctional lipids were generated under these conditions, the analysis also revealed labeled proteins with similar migration behavior. The proteomic analysis of protein–lipid complexes was performed as described in the Supporting Information. Proteins that revealed a 4-fold enrichment of spectral counts in pacSph/UV or pacFA/UV-treated cells compared to the non-UV irradiated control samples were considered as protein–lipid conjugates. Three independent experiments yielded a total of 1076 proteins in pacFA/+UV treated cells and 1259 proteins in pacSph/+UV treated cells (Figure S8e and Table S1). Acylation of proteins with pacFA was limited due to the short labeling time of 1 h (Figure S8f and g). This is in agreement with previous observations.¹³ Depending on the number of identifications (*n*) in the three experiments, identified protein–lipid complexes were clustered into high- (*n* = 3), medium- (*n* = 2), and low- (*n* = 1) confidence complexes. Three independent experiments led to the identification of 223 high confidence protein–lipid complexes for pacFA/+UV and 186 for pacSph/+UV, respectively (Figure S8e). Figure 4b shows spectral counts of these proteins as a heat map. Surprisingly, although pacFA and pacSph gave rise to different subsets of bifunctional lipids, our proteomic analysis revealed a substantial overlap of protein–lipid complexes that were identified in both, pacFA/+UV and

pacSph/+UV treated cells. This is in line with the observation that the analysis by in-gel fluorescence yielded similar patterns of fluorescence labeled proteins (Figure S8c). High confidence complexes captured in pacFA/+UV treated cells revealed enrichment in mitochondrial and ER residing proteins, coinciding with the observed reticular staining of protein–lipid complexes (Figure 4c and d). The identification of mitochondrial fatty acid handling machinery, mediating their transport (carnitine O-palmitoyltransferase 2) or being involved in their degradation (acyl-Coenzyme A dehydrogenase, long-chain-fatty-acid-CoA ligase 1) suggests an active metabolism of pacFA. Examples of identified ER resident proteins are the GPI transamidase component PIG-S, required for the biosynthesis of GPI-anchored proteins, or the monoacyl glycerol lipase. This is also reflected in our automated analysis of GO-terms of high confidence proteins derived from pacFA/+UV treated cells, which revealed an enrichment for proteins involved in the biosynthesis and degradation of fatty acids as well as for ER and mitochondrial proteins (Figure S9). In contrast, protein–sphingolipid complexes revealed a broader distribution of subcellular localizations. Proteins exclusively identified in pacSph/+UV treated cells were enriched in lysosomal and plasma membrane residing proteins (Figure 4c). This is in agreement with the observed colocalization of protein–sphingolipid complexes with lysosomal structures as well as with our GO-term analysis (Figure 4d). Many of the complexes identified from pacSph/+UV treated cells were found to have a functional relationship to sphingolipids (Table S2). Examples thereof are shown in Figure 4e and include bona fide sphingolipid-handling proteins such as the ceramide synthase 2 (CERS2), cathepsin D (CTSD), glucosylceramidase (GBA) and beta-galactosidase (GLB1), demonstrating the feasibility of our method in tracking down novel sphingolipid-handling machinery.

Validation of Protein–Lipid Interactions. To demonstrate the application of pacSph to other cell lines, we generated a S1PL knock out in HeLa cells using the CRISPR system (S1PL^{-/-} HeLa, unpublished) and found exclusive incorporation of pacSph into sphingolipids when administered to the cells (Figure S10a). Employing this cell line, we validated seven protein–sphingolipid interactions, including the known sphingolipid-binding proteins p24 and GPAA1,^{10,33} as well as five novel candidate proteins: Palmitoyl-protein thioesterase 1 (PPT1), putative phospholipase B-like 2 (PLBD2), translocon-associated protein subunit alpha (SSR1), heparan sulfate 2-O-sulfotransferase 1 (HS2ST1), and basigin (BSG). We transiently expressed the respective FLAG-tagged human homologues and treated the cells with 6 μ M pacSph or 100 μ M pacFA for 4 h, following UV-irradiation and then subjected the lysates to click reactions with biotin-azide. Biotinylated proteins were enriched and analyzed by SDS-PAGE and Western blotting.

In line with our proteomic identification, we observed exclusive binding of the lysosomal candidate proteins PLBD2 and PPT1 to sphingolipids (Figure 4f). To rule out that the interactions of these proteins with sphingolipids were a result of the pronounced localization of bifunctional sphingolipids in lysosomal structures, we employed NPC2, a lysosomal cholesterol transfer protein. No cross-linked product was observed when cells were pacFA/+UV or pacSph/+UV treated. We then employed SEC14l2, which has previously been reported to bind to the glycerophospholipids phosphatidylglycerol, phosphatidylserine, phosphatidylinositol, and phosphati-

dic acid in cross-linking experiments.³⁴ In line with these findings, we found SEC14l2 to exclusively cross-link to bifunctional glycerolipids, but not sphingolipids.

Next, we investigated various transmembrane-spanning proteins including the “sphingolipid-binding motif” containing proteins p24 and GPAA1 as well as SSR1, HS2ST1, and BSG. In line with our proteomic analysis, all proteins gave rise to cross-linked products with both sphingolipids and glycerolipids (Figure 4f). As a negative control for protein–sphingolipid interactions, we used ASGR1, which is lacking the sphingolipid-binding motif of p24 and GPAA1 but is exposed to the bulk pool of cellular sphingolipids at the plasma membrane.³³ No cross-linked product of ASGR1 with sphingolipids was observed. Interestingly, we observed a slower migration behavior of nearly all membrane spanning proteins in pacFA/+UV treated cells, which was not observed in pacSph/+UV-treated cells. We concluded that the copy numbers of bifunctional glycerolipids exceeded those of the overexpressed FLAG-tagged candidate proteins, which is likely to result in an unspecific labeling and might explain the observed overlap of protein–lipid complexes in our proteomic analysis. Our quantitative analysis of bifunctional lipid levels revealed that total bifunctional sphingolipid levels were more than 2-fold lower compared with bifunctional glycerolipid levels. As pacFA was predominantly ($\geq 50\%$) incorporated into PC, individual bifunctional sphingolipids showed 3- (Sph) to 5-fold (Cer, SM), and even up to 24-fold (GlcCer), lower copy numbers compared with pacPC (Figure S10a–c). Therefore, we went on and addressed the specificity of protein–sphingolipid complex formation in competition experiments in which cells were fed with 0.5 μM pacSph in the absence or presence of a 10-fold excess of natural sphingosine. For four out of five tested proteins, we found protein–sphingolipid complex formation to be sensitive under these conditions (Figure 4g). To further address specificity and to investigate the nature of the lipids bound to proteins, we performed cross-link experiments in which we dissected the *de novo* biosynthesis of sphingolipids employing FB1 (Figure 4h). The latter resulted in reduced cross-link efficiency for the SM-binding protein p24 as well as for GPAA1, HS2ST1, and SSR1, suggesting that these proteins do not interact with pacSph itself but with a metabolite of pacSph.

Specificity. For the proteomic profiling of protein–sphingolipid complexes, we initially reasoned that pacFA, which is predominantly incorporated into PC will serve as a control to address specificity of protein–sphingolipid interactions. The pronounced overlap of protein–glycerolipid with protein–sphingolipid complexes in our proteomic analysis, as well as the observed shift in the migration behavior of protein–glycerolipid complexes raises the question of whether pacFA is an appropriate control to address specificity. As both precursors give rise to various metabolites with different copy numbers and localizations, different bifunctional lipid classes will not serve as a generic control in global screens for protein–lipid interactions. While unspecific cross-linking, due to high copy numbers of individual bifunctional glycerolipids, might be a reason for the observed overlap in our proteomic screen, other factors need to be taken into consideration: (i) the abundance of PC in the lipid shell of integral membrane proteins, a phenomenon which has been previously observed for p24;¹⁰ (ii) the occurrence of two or multiple lipid-binding sites within proteins;³⁵ as well as (iii) the possibility that a single lipid-binding site may recognize multiple lipids. The latter is

exemplified by the identification of the phosphatidylinositol transfer protein β (PITBNB), which was shown to transfer the glycerophospholipids PC and PI, as well as the sphingolipid SM and thus explains its identification in pacFA/+UV as well as pacSph/+UV treated cells.^{36,37} Additionally, (iv) although pacSph and its derived metabolites seem to closely mimic their natural counterparts, it cannot be excluded that the functional groups alter the physicochemical properties of the bifunctionalized sphingolipids.

Despite lowering the concentration of pacSph more than 10-fold, we were able to capture known as well as novel protein–sphingolipid complexes, which were sensitive in competition experiments, as well as in experiments with a dissected sphingolipid biosynthetic pathway. The ability to manipulate (bifunctional) sphingolipid levels will enable following the dynamics of protein–sphingolipid complex formations on a global scale. Although we could not identify bifunctional sphingolipids to be formed when feeding pacFA to cells, their levels might be below the detection limit. Dissecting the biosynthetic pathway of sphingolipids would also allow to test whether protein–lipid conjugates, which were obtained with pacFA, are sensitive under these conditions. One major challenge with the presented approach is to identify the nature of the cross-linked lipid.³⁸ Here, the ability to dissect the *de novo* synthetic pathway of bifunctional sphingolipids provides means for the identification of proteins interacting with subsets thereof.

We also like to mention limitations of the presented technology. The nonstereospecific reduction of protected keto-pacSph and its subsequent deprotection yields the two diastereomers *erythro*- and *threo*-pacSph. While pure *erythro*-pacSph was isolated with a yield of 90%, *threo*-pacSph could not be isolated in a pure form. The observed rapid conversion of extracellular provided sphingosine analogs and their incorporation into other lipid classes limits the applications of pacSph to S1PL knock out cell lines. The rapidly growing area of genome editing, however, will enable the application of pacSph to other cellular systems and model organisms.³⁹ It is noteworthy that such genetically modified systems might have altered metabolic states.

In summary, we have established and characterized a novel bifunctional lipid precursor for the global profiling of protein–sphingolipid interactions in living cells. For the first time, we have combined a quantitative analysis of *de novo* synthesized sphingolipids with the imaging and proteomic analysis of their interacting proteins. This allows the metabolic flux of *de novo* synthesized sphingolipids to be followed in time and space and will permit new insights into the transport and metabolism of sphingolipids upon targeting of lipid-handling machinery. The presented technology will help to identify putative therapeutic drug targets in sphingolipid-related diseases.

ASSOCIATED CONTENT

S Supporting Information

The Supporting Information is available free of charge on the ACS Publications website at DOI: 10.1021/acscchembio.5b00810.

Materials and methods, Figures S1–S10, and Table S2
(PDF)

Table S1 (XLSX)

AUTHOR INFORMATION

Corresponding Authors

*Phone: +31 71 527-6458. E-mail: per.haberkant@gmail.com.
 *Phone: +49 6221 387-8210. E-mail: schultz@embl.de.

Present Address

[#]Leiden University, Leiden Institute of Chemistry, Department Biochemistry, Einsteinweg 55, 2333 CC Leiden, The Netherlands

Notes

The authors declare no competing financial interest.

ACKNOWLEDGMENTS

We thank J. Kirkpatrick, the Proteomics Core Facility at EMBL, Z. Rogon (Centre for Biomolecular Network Analysis at EMBL), and T. Sachsenheimer for technical assistance. We thank K. Simons for critical reading and comments on the manuscript. P.H. is a fellow of the EMBL Interdisciplinary Postdoc (EIPOD) under Marie Curie Actions Cofund. This work was supported by the European Union seventh FP Marie-Curie ITN "SPHINCONET" (C.S. and D.H.) and TRR83 of the DFG (B.B., C.S.).

REFERENCES

- (1) Wenk, M. R. (2010) Lipidomics: new tools and applications. *Cell* **143**, 888–895.
- (2) Lingwood, D., and Simons, K. (2010) Lipid rafts as a membrane-organizing principle. *Science* **327**, 46–50.
- (3) Simons, K., and Gerl, M. J. (2010) Revitalizing membrane rafts: new tools and insights. *Nat. Rev. Mol. Cell Biol.* **11**, 688–699.
- (4) Honigmann, A., Mueller, V., Ta, H., Schoenle, A., Sezgin, E., Hell, S. W., and Eggeling, C. (2014) Scanning STED-FCS reveals spatiotemporal heterogeneity of lipid interaction in the plasma membrane of living cells. *Nat. Commun.* **5**, 5412.
- (5) Hiramoto-Yamaki, N., Tanaka, K. A., Suzuki, K. G., Hirosawa, K. M., Miyahara, M. S., Kalay, Z., Tanaka, K., Kasai, R. S., Kusumi, A., and Fujiwara, T. K. (2014) Ultrafast diffusion of a fluorescent cholesterol analog in compartmentalized plasma membranes. *Traffic* **15**, 583–612.
- (6) Frisz, J. F., Klitzing, H. A., Lou, K., Hutcheon, I. D., Weber, P. K., Zimmerberg, J., and Kraft, M. L. (2013) Sphingolipid domains in the plasma membranes of fibroblasts are not enriched with cholesterol. *J. Biol. Chem.* **288**, 16855–16861.
- (7) Hannun, Y. A., and Obeid, L. M. (2008) Principles of bioactive lipid signalling: lessons from sphingolipids. *Nat. Rev. Mol. Cell Biol.* **9**, 139–150.
- (8) Hla, T., and Dannenberg, A. J. (2012) Sphingolipid signaling in metabolic disorders. *Cell Metab.* **16**, 420–434.
- (9) Wennekes, T., van den Berg, R. J., Boot, R. G., van der Marel, G. A., Overkleft, H. S., and Aerts, J. M. (2009) Glycosphingolipids—nature, function, and pharmacological modulation. *Angew. Chem., Int. Ed.* **48**, 8848–8869.
- (10) Contreras, F. X., Ernst, A. M., Haberkant, P., Bjorkholm, P., Lindahl, E., Gonen, B., Tischer, C., Elofsson, A., von Heijne, G., Thiele, C., Pepperkok, R., Wieland, F., and Brugge, B. (2012) Molecular recognition of a single sphingolipid species by a protein's transmembrane domain. *Nature* **481**, 525–529.
- (11) Snook, C. F., Jones, J. A., and Hannun, Y. A. (2006) Sphingolipid-binding proteins. *Biochim. Biophys. Acta, Mol. Cell Biol. Lipids* **1761**, 927–946.
- (12) Brinkmann, V., Billich, A., Baumruker, T., Heining, P., Schmouder, R., Francis, G., Aradhya, S., and Burtin, P. (2010) Fingolimod (FTY720): discovery and development of an oral drug to treat multiple sclerosis. *Nat. Rev. Drug Discovery* **9**, 883–897.
- (13) Haberkant, P., Raijmakers, R., Wildwater, M., Sachsenheimer, T., Brugge, B., Maeda, K., Houweling, M., Gavin, A. C., Schultz, C., van Meer, G., Heck, A. J., and Holthuis, J. C. (2013) In vivo profiling and visualization of cellular protein-lipid interactions using bifunctional fatty acids. *Angew. Chem., Int. Ed.* **52**, 4033–4038.
- (14) Hulce, J. J., Cognetta, A. B., Niphakis, M. J., Tully, S. E., and Cravatt, B. F. (2013) Proteome-wide mapping of cholesterol-interacting proteins in mammalian cells. *Nat. Methods* **10**, 259–264.
- (15) Haberkant, P., and Holthuis, J. C. (2014) Fat & fabulous: bifunctional lipids in the spotlight. *Biochim. Biophys. Acta, Mol. Cell Biol. Lipids* **1841**, 1022–1030.
- (16) Niphakis, M. J., Lum, K. M., Cognetta, A. B., Correia, B. E., Ichu, T. A., Olucha, J., Brown, S. J., Kundu, S., Piscitelli, F., Rosen, H., and Cravatt, B. F. (2015) A Global Map of Lipid-Binding Proteins and Their Ligandability in Cells. *Cell* **161**, 1668–1680.
- (17) Haberkant, P., Schmitt, O., Contreras, F. X., Thiele, C., Hanada, K., Sprong, H., Reinhard, C., Wieland, F. T., and Brügger, B. (2008) Protein-sphingolipid interactions within cellular membranes. *J. Lipid Res.* **49**, 251–262.
- (18) Thiele, C., Papan, C., Hoelper, D., Kusserow, K., Gaebler, A., Schoene, M., Piotrowitz, K., Lohmann, D., Spandl, J., Stevanovic, A., Shevchenko, A., and Kuerschner, L. (2012) Tracing Fatty Acid Metabolism by Click Chemistry. *ACS Chem. Biol.* **7**, 2004–2011.
- (19) Kim, R., Lou, K., and Kraft, M. L. (2013) A new, long-wavelength borondipyromethene sphingosine for studying sphingolipid dynamics in live cells. *J. Lipid Res.* **54**, 265–275.
- (20) Riboni, L., Bassi, R., Prinetti, A., Viani, P., and Tettamanti, G. (1999) Predominance of the acylation route in the metabolic processing of exogenous sphingosine in neural and extraneuronal cells in culture. *Biochem. J.* **338** (Pt 1), 147–151.
- (21) Serra, M., and Saba, J. D. (2010) Sphingosine 1-phosphate lyase, a key regulator of sphingosine 1-phosphate signaling and function. *Adv. Enzyme Regul.* **50**, 349–362.
- (22) Van Veldhoven, P. P., and Mannaerts, G. P. (1991) Subcellular localization and membrane topology of sphingosine-1-phosphate lyase in rat liver. *J. Biol. Chem.* **266**, 12502–12507.
- (23) Stoffel, W., and Sticht, G. (1967) Metabolism of sphingosine bases, II. Studies on the degradation and transformation of [3–14C]erythro-DL-dihydroosphingosine, [7–3H]erythro-DL-sphingosine, [5–3H]threo-L-dihydroosphingosine and [3–14C;1–3H]erythro-DL-dihydroosphingosine in rat liver. *Hoppe-Seyler's Z. Physiol. Chem.* **348**, 1345–1351.
- (24) Nakahara, K., Ohkuni, A., Kitamura, T., Abe, K., Naganuma, T., Ohno, Y., Zoeller, R. A., and Kihara, A. (2012) The Sjögren-Larsson syndrome gene encodes a hexadecenal dehydrogenase of the sphingosine 1-phosphate degradation pathway. *Mol. Cell* **46**, 461–471.
- (25) Colie, S., Van Veldhoven, P. P., Kedjouar, B., Bedia, C., Albinet, V., Sorli, S. C., Garcia, V., Djavaheri-Mergny, M., Bauvy, C., Codogno, P., Levade, T., and Andrieu-Abadie, N. (2009) Disruption of sphingosine 1-phosphate lyase confers resistance to chemotherapy and promotes oncogenesis through Bcl-2/Bcl-xL upregulation. *Cancer Res.* **69**, 9346–9353.
- (26) Wang, E., Norred, W. P., Bacon, C. W., Riley, R. T., and Merrill, A. H., Jr. (1991) Inhibition of sphingolipid biosynthesis by fumonisins. Implications for diseases associated with Fusarium moniliforme. *J. Biol. Chem.* **266**, 14486–14490.
- (27) Rao Vunnam, R., and Radin, N. S. (1980) Analogs of ceramide that inhibit glucocerebroside synthetase in mouse brain. *Chem. Phys. Lipids* **26**, 265–278.
- (28) Levy, M., and Futerman, A. H. (2010) Mammalian ceramide synthases. *IUBMB Life* **62**, 347–356.
- (29) van Meer, G., and Lisman, Q. (2002) Sphingolipid transport: rafts and translocators. *J. Biol. Chem.* **277**, 25855–25858.
- (30) Halter, D., Neumann, S., van Dijk, S. M., Wolthoorn, J., de Maziere, A. M., Vieira, O. V., Mattjus, P., Klumperman, J., van Meer, G., and Sprong, H. (2007) Pre- and post-Golgi translocation of glucosylceramide in glycosphingolipid synthesis. *J. Cell Biol.* **179**, 101–115.
- (31) Huitema, K., van den Dikkenberg, J., Brouwers, J. F., and Holthuis, J. C. (2004) Identification of a family of animal sphingomyelin synthases. *EMBO J.* **23**, 33–44.

- (32) van Meer, G., Voelker, D. R., and Feigenson, G. W. (2008) Membrane lipids: where they are and how they behave. *Nat. Rev. Mol. Cell Biol.* 9, 112–124.
- (33) Bjorkholm, P., Ernst, A. M., Hacke, M., Wieland, F., Brugger, B., and von Heijne, G. (2014) Identification of novel sphingolipid-binding motifs in mammalian membrane proteins. *Biochim. Biophys. Acta, Biomembr.* 1838, 2066–2070.
- (34) Caras, I. W., Friedlander, E. J., and Bloch, K. (1980) Interactions of supernatant protein factor with components of the microsomal squalene epoxidase system. Binding of supernatant protein factor to anionic phospholipids. *J. Biol. Chem.* 255, 3575–3580.
- (35) Gallego, O., Betts, M. J., Gvozdenovic-Jeremic, J., Maeda, K., Matetzki, C., Aguilar-Gurrieri, C., Beltran-Alvarez, P., Bonn, S., Fernandez-Tornero, C., Jensen, L. J., Kuhn, M., Trott, J., Rybin, V., Muller, C. W., Bork, P., Kaksonen, M., Russell, R. B., and Gavin, A. C. (2010) A systematic screen for protein-lipid interactions in *Saccharomyces cerevisiae*. *Mol. Syst. Biol.* 6, 430.
- (36) Wirtz, K. W. (1997) Phospholipid transfer proteins revisited. *Biochem. J.* 324 (Pt 2), 353–360.
- (37) Vordtriede, P. B., Doan, C. N., Tremblay, J. M., Helmkamp, G. M., Jr., and Yoder, M. D. (2005) Structure of PITP β in complex with phosphatidylcholine: comparison of structure and lipid transfer to other PITP isoforms. *Biochemistry* 44, 14760–14771.
- (38) Gerl, M. J., Sachsenheimer, T., Grzybek, M., Coskun, U., Wieland, F. T., and Brugger, B. (2014) Analysis of transmembrane domains and lipid modified peptides with matrix-assisted laser desorption ionization-time-of-flight mass spectrometry. *Anal. Chem.* 86, 3722–3726.
- (39) Sakuma, T., and Woltjen, K. (2014) Nuclease-mediated genome editing: At the front-line of functional genomics technology. *Dev Growth Differ* 56, 2–13.